Received: 16 August 2021 | Revised: 28 March 2022 | Accepted: 29 March 2022

DOI: 10.1002/joc.7636

RESEARCH ARTICLE

International Journal of Climatology RMetS

Changes in heat stress considering temperature, humidity, and wind over East Asia under RCP8.5 and SSP5-8.5 scenarios

Ana Juzbašić[1] | **Joong-Bae Ahn**[1] | **Dong-Hyun Cha**[2] | **Eun-Chul Chang**[3] | **Seung-Ki Min**[4]

[1]Department of Atmospheric Sciences, Pusan National University, Busan, South Korea

[2]Ulsan National Institute of Science and Technology, Ulsan, South Korea

[3]Kongju National University, Gongju, South Korea

[4]Pohang University of Science and Technology, Pohang, South Korea

Correspondence
Joong-Bae Ahn, Department of Atmospheric Sciences, Pusan National University, Busan, South Korea.
Email: jbahn@pusan.ac.kr

Funding information
Korea Meteorological Administration Research and Development, Grant/Award Number: KMI2020-01411

Abstract

The net effective temperature (NET), an index that includes the combined effects of temperature, humidity, and wind, was used along with temperature to assess the impacts of climate change on the heat stress perception in East Asia, one of the regions considered most vulnerable to heat stress. The need for dynamic downscaling has been emphasized because the regional effects of climate change do not follow the global levels linearly. In this study, daily maximums calculated from the 3-hourly data downscaled by five different regional climate models from four coupled general circulation models participating in Coordinated Regional Climate Downscaling Experiment-East Asia phase 2 were utilized. To account for the fact human beings acclimate to their environments, 95th percentile of the maximum temperature and maximum NET was used along with the average boreal summer maximum temperatures/NETs. The performance of the models was assessed first, which showed that the models reproduced the current climate well. Future projections revealed an increase in both average and 95th percentile of the maximum temperature and NET over the entire domain for both the RCP8.5 and SSP5-8.5 scenarios. The increase in heat stress (NET) was slightly larger than the temperature itself, with an increase of up to 7/10°C for temperature and 8/11°C for NET in RCP8.5/SSP5-8.5, respectively. The overall increases in temperature and NET were projected to be higher in the higher latitudes, while the increase in the frequency of the temperature and NET extremes was predicted to be higher in the already vulnerable regions in the southern part of the domain.

KEYWORDS

climate change, heat stress, multimodel, RCP scenarios, SSP scenarios

1 | INTRODUCTION

According to the Intergovernmental Panel on Climate Change (IPCC) reports (IPCC, 2007; 2014), worldwide-observed global warming is most likely a consequence of the anthropogenic increase in greenhouse gases. Human emissions are currently the highest in history (Ritchie and Roser, 2020), and the resulting climate change has and will have significant effects on ecosystems and human lives. Changes in temperature extremes and heat waves have been observed globally, particularly in Asia, Europe, and Australia (IPCC AR5). East Asia is one of the most vulnerable areas for climate change, owing to several natural and anthropogenic factors, such as topography and population density (Prajapat *et al*., 2019 and Im *et al*., 2017 for India; Lee and Min, 2018 and Jo *et al*., 2020 for South Korea).

The human experience of heat depends on many factors that affect heat exchange between human beings and the environment. There are simple formulas for the feeling of heat, which usually include temperature and humidity, for example, indoor apparent temperature (Steadman, 1984), wet bulb temperature (Stull, 2011), and other heat indices (e.g., Diffenbaugh *et al*., 2007). Their main advantage is being easy to calculate using existing data. On the other hand, very complicated bioclimatic indices such as the Universal Thermal Climate Index (UTCI; Blazejczyk *et al*., 2011) and physiological equivalent temperature (Höppe, 1999) provide detailed data, but they either require complicated technology to acquire the necessary measurements or are complicated to calculate. The net effective temperature (NET), which was developed as the effective temperature (ET) by Missenard (1937) and updated by WMO in 1972 to include wind, is an index that includes temperature, humidity, and wind. These parameters can be obtained easily from both measurements and model outputs while having comparable performance to the more complicated indices, such as UTCI (Blazejczyk *et al*., 2011). While some of the more complicated indices can be obtained from model projections by applying certain assumptions, they require greater number of variables than NET, as well as observational data which is often not available. For example, wet bulb globe temperature (WBGT) has been used to assess heat stress projection before (Suzuki-Parker and Kusaka, 2016), but WBGT calculations include measuring or estimating globe temperature. Formulas to estimate globe temperature are usually made by fitting the model data to the observational data, and therefore these formulas are not always applicable on larger domains or for all conditions (Okada and Kusaka, 2013). UTCI calculation, on the other hand, involves either several time-consuming steps, or the polynomial regression which is not as accurate. The UTCI calculation errors are around 1.2 K when wind speeds of over 20 $m \cdot s^{-1}$ are excluded, which could be considered an acceptable level (Bröde *et al*., 2012), but when the errors in the model performance of each variable are taken into account, using NET is most reasonable given the simplicity of calculations and comparable performance to UTCI.

The most common way to assess the impact of future climate change on human lives is using coupled general circulation models (CGCMs). CGCMs provide a good overall picture but are unsuitable for the regional impacts because of the relatively low resolution (100–300 km). Therefore, regional climate models (RCMs) are used widely to dynamically downscale the CGCM output over regions of complex topography (i.e., Park *et al*., 2016; Zou and Zhou, 2016; Im *et al*., 2017; Jo *et al*., 2019). Several previous studies have shown that there is added value in RCM simulations when analysing regions of complex topography, islands, and coastal regions, which comprise large parts of domain analysed in this study. In addition, the added value of RCMs is even more visible in the simulation of the extremes and tail-ends of the distributions (e.g., Lee and Hong, 2014; Ciarlo *et al*., 2021), which is what we have analysed in this study. The main aims of the Coordinated Regional Climate Downscaling Experiment (CORDEX; https://cordex.org/) are to obtain the added value by improving the resolution, both spatial and temporal, which enables a better reproduction of extreme values, and to reduce the model uncertainty by using a multiple-model ensemble in simulating regional climate. In particular, when assessing the impact of climate extremes, it is essential to use several models because the uncertainties in those changes are larger than in changes in the mean values.

The CORDEX-EA (East Asia) phase 2 domain covers most areas of Asia vulnerable to extreme heat. Several studies assessed the impacts of changes in climate extremes over East Asia using regional models (Oh *et al*., 2014; Ahn *et al*., 2016; Ngo-Duc *et al*., 2016; Park and Min, 2019), but they focused only on the direct model output variables, such as temperature and precipitation. Some previous studies also approximated the regional effects of heat stress using the indices based on temperature and humidity (e.g., Casanueva *et al*., 2019, for Europe using the wet-bulb globe temperature with constant wind and radiation assumption; Sylla *et al*., 2018, for West Africa using the National Oceanic and Atmospheric Administration/National Weather Service heat index; Im *et al*., 2017; for South Asia using the wet-bulb temperature).

On the other hand, there is a paucity of studies for the whole East Asia domain, which take wind and human adaptability into account when addressing heat stress while simultaneously using multi CGCM-RCM chains. This study assesses the changes in heat stress defined by temperature, humidity, and wind using the fine resolution 3-hourly data from a large number of CGCM-RCM chains. Hence, detailed analyses of projected changes over the whole East Asia domain could be performed.

2 | DATA AND METHODS

2.1 | Data

Dynamical downscaling of the four CGCMs from Coupled Model Intercomparison Project (CMIP) phases 5 and 6 has been done under the national framework in South Korea. In total, 10 CGCM-RCM chains were used in the present study. Three of the CGCMs used are part of CMIP phase 5: Earth System Model from the Geophysical Fluid Dynamics Laboratory (GFDL-ESM-2M; Dunne *et al*., 2012), Max Planck Institute Earth System Model Low Resolution (MPI-ESM-LR; Giorgetta *et al*., 2013), and Hadley Centre Global Environment Model version 2 – Atmosphere–Ocean (HadGEM2-AO; Martin *et al*., 2011) and one model is part of CMIP phase 6: UK Earth System Model (UKESM; Sellar *et al*., 2019). Table 1 lists the RCMs used, their parameterizations and resolutions, CGCM-RCM chains, and the institutions producing the downscaled data. In addition, all RCMs use spectral nudging.

This study used the following three simulations: historical, which spans 1981–2005, and two future simulations, which span 2081–2099. The future simulations were based on representative concentration pathway (RCP) scenario RCP8.5 for models from CMIP5 and shared socioeconomic pathway 5 based on RCP8.5 (SSP5-8.5) for the model from CMIP6. Based on the scenarios they use, the models were split into two groups, and an ensemble was done for each group separately, hereafter called "CMIP5_ens" and "CMIP6_ens." The reason for using 2099 instead of standard 2100 as a final year is purely technical because some of the CGCM-RCM chains used only have model output until January 1, 2100.

For model validation, JRA-55 (Japan Meteorological Agency, 2013) data was used for the domain of 75°–180°E, 0°–50°N, which roughly corresponds to the CORDEX-EA2 domain. The variables used were the gridded near-surface temperature, near-surface humidity, and near-surface wind in the 3-hourly time and 55 km horizontal resolution. Given that the downscaled model data has a finer resolution than the JRA-55 data, it is expected it will be sufficient to describe the regional changes in the heat stress-related extremes. JRA-55 is the third-generation reanalysis that uses the full observation system and is in good accordance with the measurements (Kobayashi *et al*., 2015). Furthermore, JRA-55 is a fine resolution dataset, which has all of the required variables (temperature, humidity, and wind) readily available. All the data used were regridded to a 0.25° × 0.25° grid for comparison purposes. Model data were regridded using simple inverse distance weighting, while JRA-55 data were regridded using conventional bilinear interpolation. As the JRA-55 data are on the rectilinear grid, and the model data are originally on the curvilinear grid, different methods had to be employed to regrid the data to the common grid.

2.2 | Methods

Two variables were used to assess the changes in the heat stress by the end of the 21st century: daily maximum temperature and the daily maximum NET. NET is a useful parameter because of several factors: it is simple to compute, easy to interpret, and consistent with the human perception of heat (Li and Chan, 2000). Although NET was used only to assess heat stress in the present study, this variable can also assess wind chill. NET formula is as follows (WMO, 1972):

$$\mathrm{NET} = 37 - \frac{37 - T}{0.68 - 0.0014RH + \frac{1}{1.76 + 1.4v^{0.75}}} - 0.29T(1 - 0.01RH),$$

where NET is the net effective temperature in °C; T is the near-surface air temperature in °C; RH is the relative humidity in %; and v is the near-surface wind speed in $\mathrm{m \cdot s^{-1}}$.

NET was calculated on a 3-hourly basis for the boreal summer period (June–July–August [JJA]). The largest contribution was from the temperature itself, and while the effects of temperature and humidity were linear, the effect of wind was nonlinear (Figure S1, Supporting Information).

World Meteorological Organization (WMO), Worth Health Organization (WHO), and United Nations Environmental Programme (UNEP) consider that temperatures over 95th percentile at specific locations can pose a threat to human health (WMO and WHO, 2015). Percentile value is used instead of absolute values to account for the fact that human beings acclimate to the climate they live in, particularly in moderate climates (Jones *et al*., 1982; Kalkstein and Davis, 1985). The daily maximum temperatures and daily maximum NET calculated from the 3-hourly values for the JJA season were used because this study focused on the summer heat stress. The 95th percentile was then calculated from these maximum values. The limitation of this approach is that the actual maximum temperatures and NETs might not be occurring at any of those times. Although the maximum temperature for a certain day exists as a model output, the NET value itself was not calculated within the models. Therefore, the same method was used for both the maximum temperature and NET for comparison and consistency.

3 | RESULTS

3.1 | Model evaluation

Figure 1 presents the Taylor diagrams for the model performance in regards to temperature. The temperature

TABLE 1 List of the CGCM-RCM chains used

RCM	CGCMs downscaled (CMIP phase)	Institution	RCM parameterizations	Resolution (lat × lon)	RCM reference
WRF v.4	GFDL-ESM2M (CMIP5) MPI-ESM-LR (CMIP5) UKESM (CMIP6)	Pusan National University (PNU)	CPS: Betts-Miller-Janjic EMS: WSM3 Radiation: Community Atmospheric Model radiation scheme(CAM) LSM: NOAH PBL: Yonsei University (YSU) PBL	25 km, 250 × 395	Powers *et al.* (2017)
RegCM v.4	GFDL-ESM2M (CMIP5)	Kongju National University (KNU)	CPS: MIT-Emanuel EMS: SUBEX Radiation: NCAR CCM3 LSM: NCAR CLM3.5 PBL: Holtslag	25 km, 249 × 394	Giorgi *et al.* (2012)
MM5 v.5	HadGEM2-AO (CMIP5) MPI-ESM-LR (CMIP5)	Ulsan National Institute of Science and Technology (UNIST)	CPS: Kain and Fritsch EMS: Reisner II Radiation: CCM2 radiative transfer scheme LSM: CLM3 PBL: YSU	25 km, 260 × 405	Grell *et al.* (1994)
CCLM v.5	HadGEM2-AO (CMIP5) MPI-ESM-LR (CMIP5) UKESM (CMIP6)	Pohang University of Science and Technology (POSTECH)	CPS: Tiedke EMS: Extended DM Radiation: Ritter and Galeyn LSM: TERRA ML PBL: Davies and Tumer	25 km, 231 × 376	Doms and Baldauf (2013)
GRIMs v.3	UKESM (CMIP6)	Kongju National University (KNU)	CPS: Simplified Arakawa-Schubert Radiation: LW: Chou, SW: Chou and Suarez LSM: NOAH LSM PBL: YSU PBL	25 km, 252 × 401	Hong *et al.* (2013)

Abbreviations: CPS, cloud parameterization scheme; LSM, land-surface model; LW, long wave; PBL, planetary boundary layer; SW, short wave.

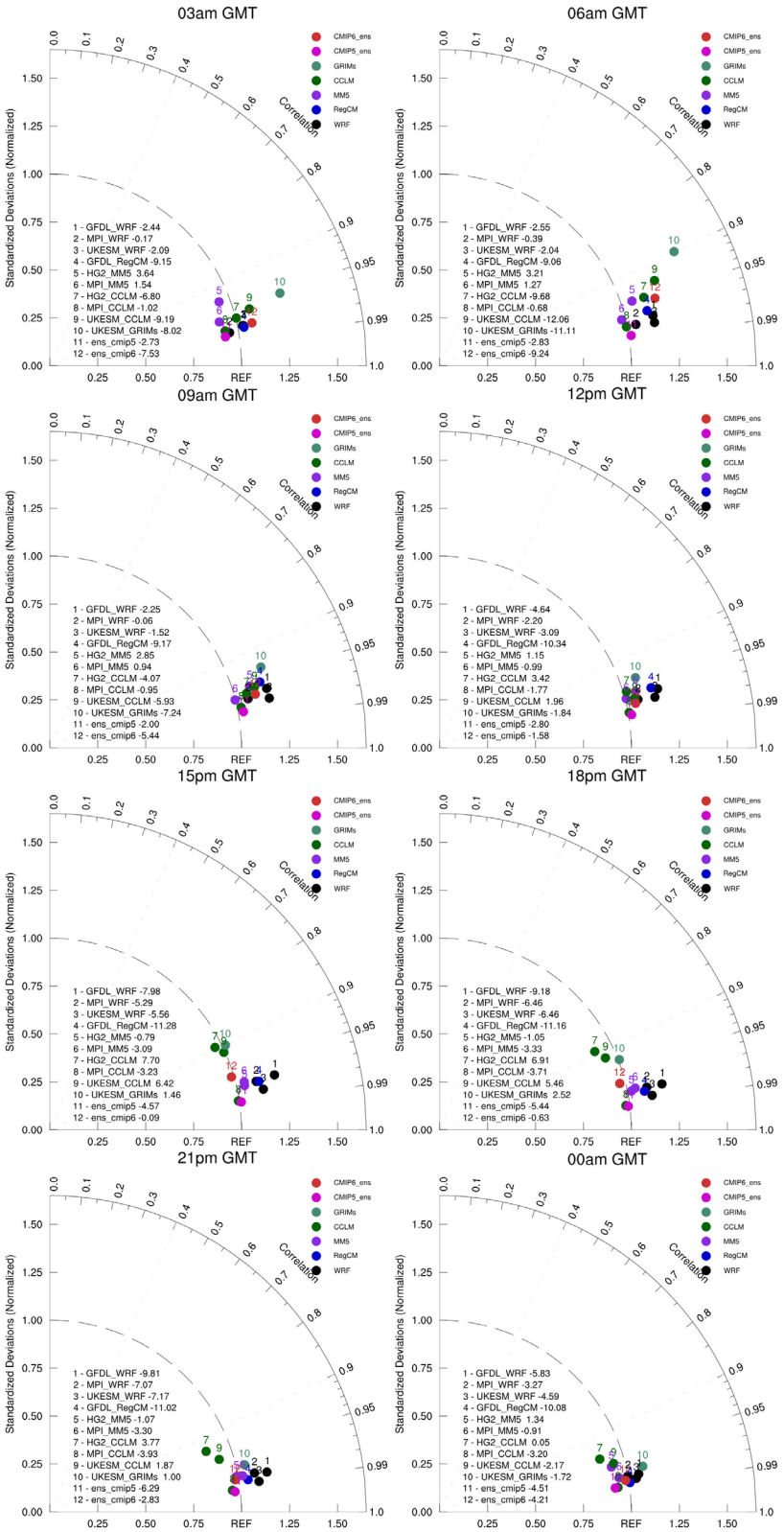

FIGURE 1 Taylor diagram showing spatial statistics of model simulations compared to the JRA-55 for the 3-hourly temperature, for the historical period. The times are denoted above each diagram. The names of the models and the respective bias % compared to JRA-55 are written on the left side of each diagram [Colour figure can be viewed at wileyonlinelibrary.com]

was simulated well in all models throughout the day in both pattern correlation and bias. The domain time zones ranged from GMT + 5.5 (India) to GMT + 9 (South Korea and Japan). Therefore, for the present research, the most important performance of the models is for 0300, 0600, 0900, and 1200 GMT (top two rows) because that is when the maximum temperatures occur. The biases depended on the time of the day and the model, and ranged from −9.19% (UKESM_CCLM) to +3.64% (HG2_MM5) for 0300 GMT, −12.06% (UKESM_CCLM) to +3.21% (HG2_MM5) for

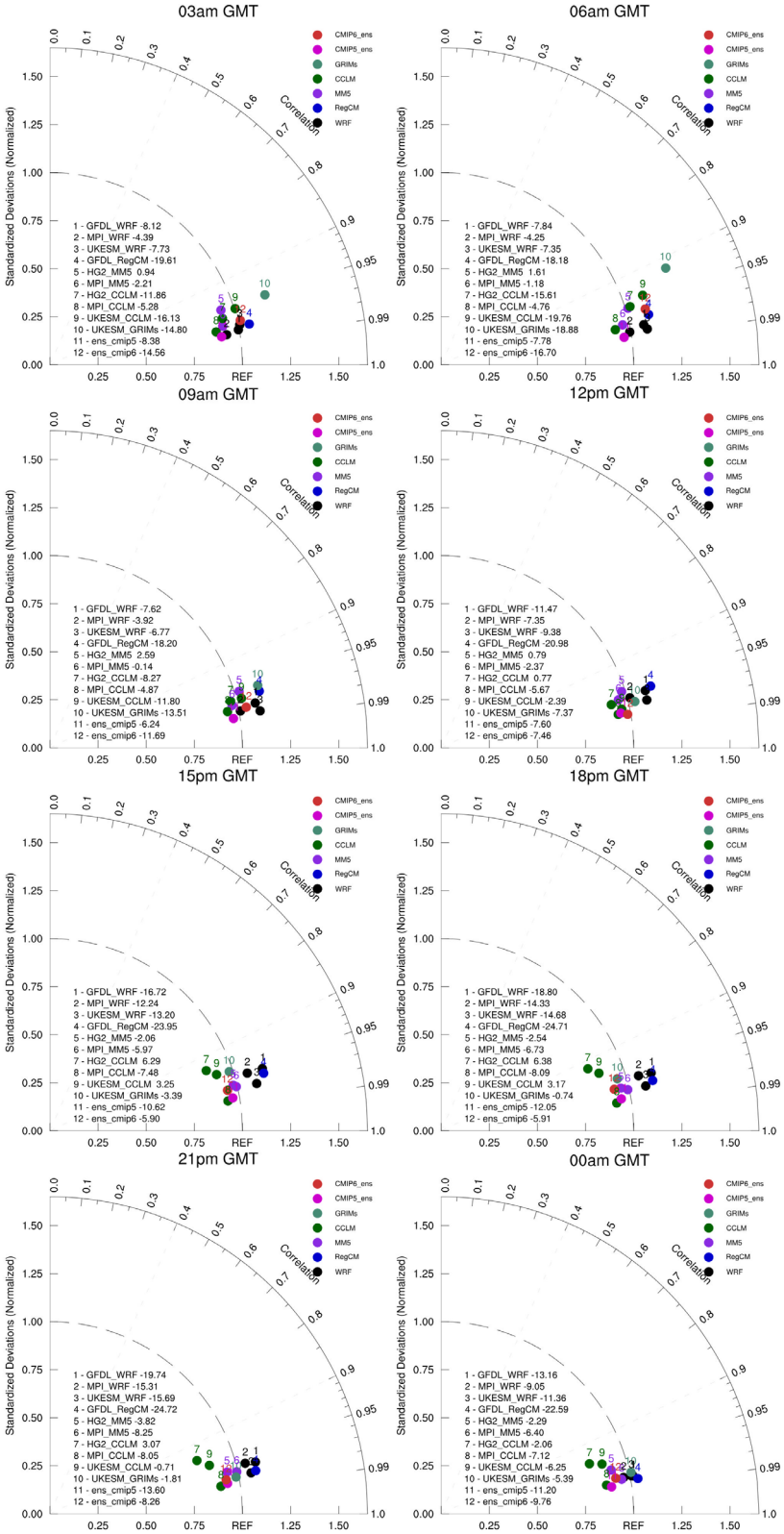

FIGURE 2 Same as Figure 1, but for NET [Colour figure can be viewed at wileyonlinelibrary.com]

0600 GMT, −9.17% (GFDL_RegCM) to −0.06% (MPI_WRF) for 0900 GMT and from −10.34 (GFDL_RegCM) to +3.42% (HG2_CCLM) for 1200 GMT. Majority of the models have bias of under 5% for these times. Interestingly, some of the models have much smaller biases during the day (e.g., all chains with WRF), some during the night (e.g., UKESM_GRIMs and UKESM_CCLM), and for some, the performance does not appear to be time-dependent. This might be due to the different radiation schemes used in the regional models. This bias appears to depend mainly on the

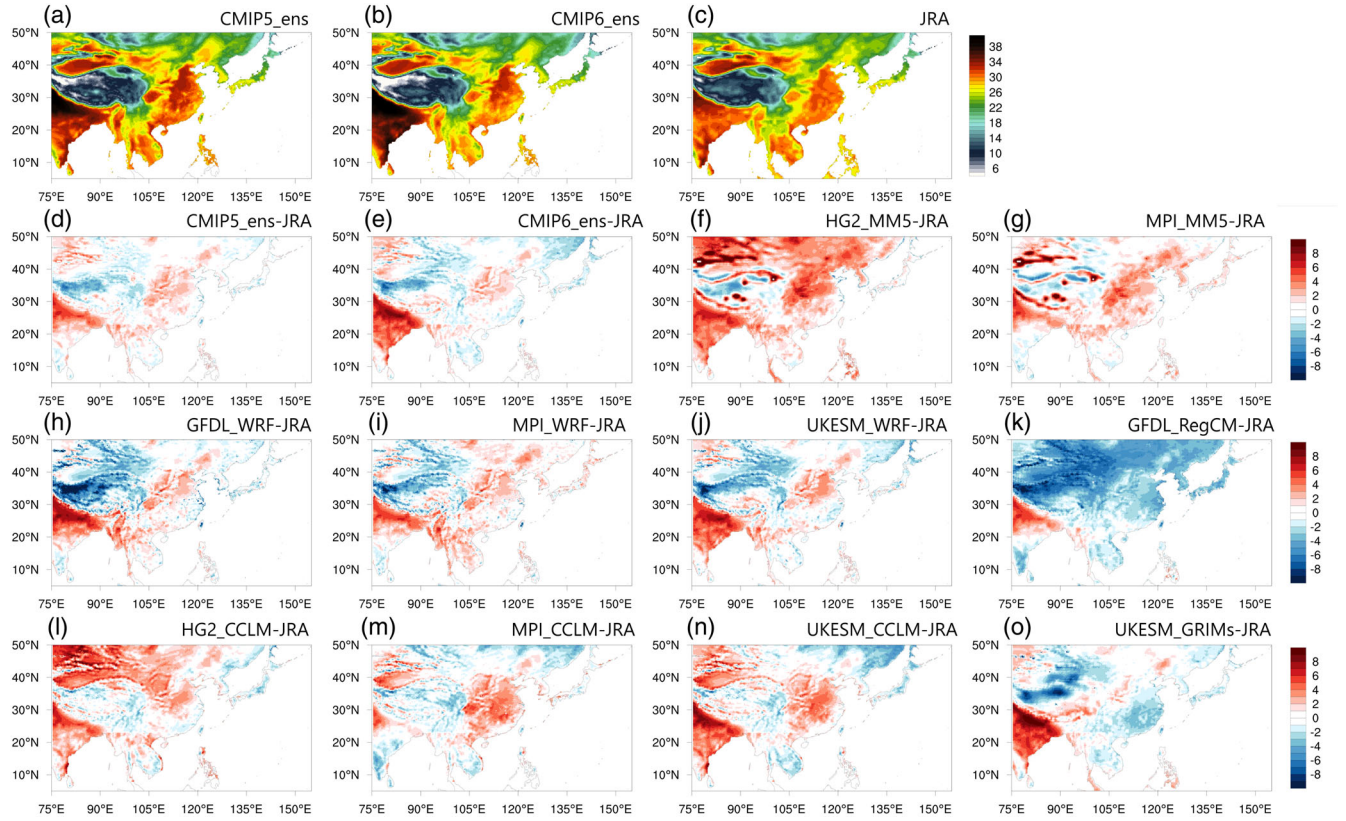

FIGURE 3 Distribution of the JJA average daily maximum temperature in °C for each ensemble (a, b), JRA-55 (c), and the bias of each ensemble (d, e) and each model separately (f–o) [Colour figure can be viewed at wileyonlinelibrary.com]

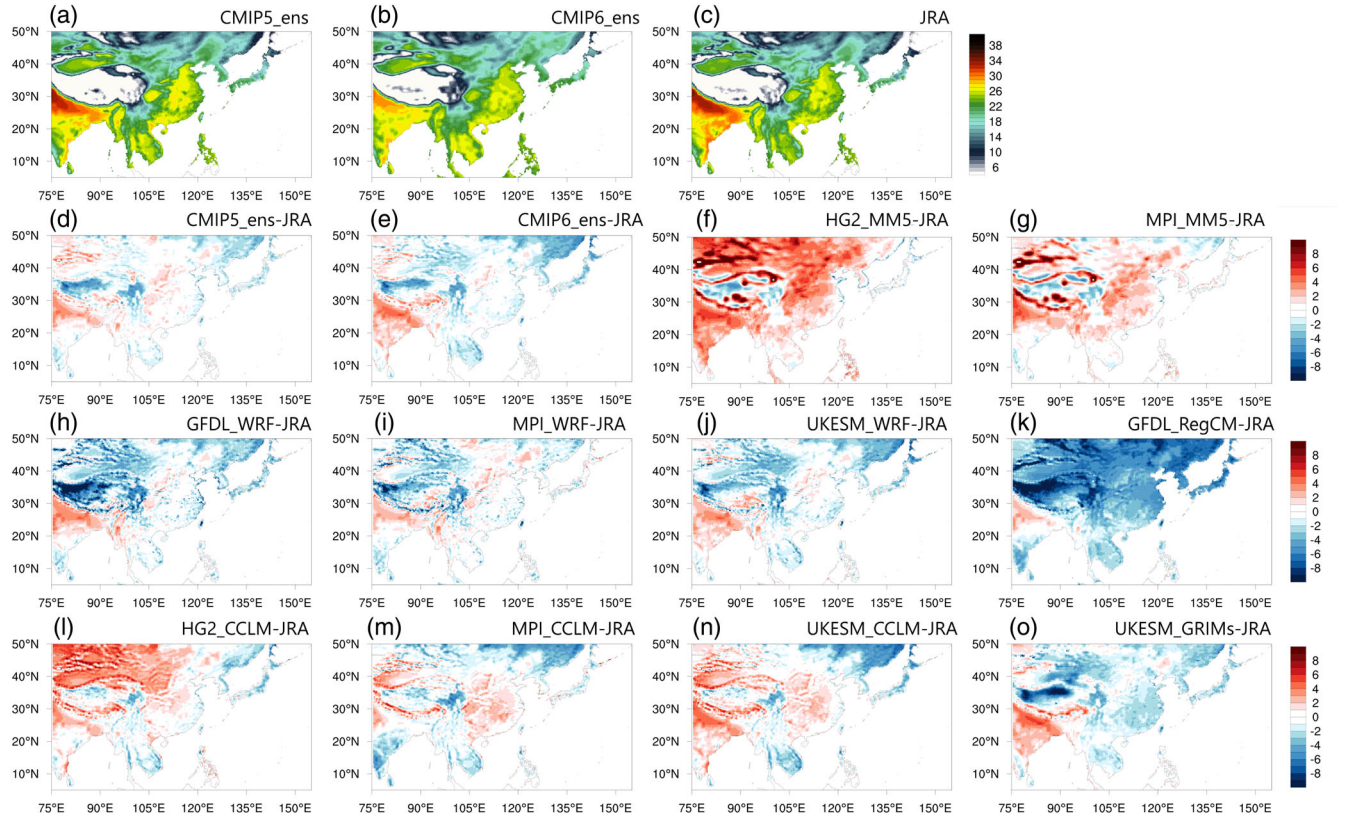

FIGURE 4 Same as Figure 3, but for NET [Colour figure can be viewed at wileyonlinelibrary.com]

choice of the RCM. On the other hand, the source of this bias is out of the scope of current research. Therefore, further studies will be needed to explain the bias and provide possible correction methods.

Models also perform well for humidity (Figure S2) and wind (Figure S3). Humidity-wise, model performance is the best during the highest heat stress times, which are important for this study (0600–1200 GMT). CMIP5_ens outperformed the majority of the individual models at all times. Wind is generally overestimated in the majority of the models (Figure S3). On the other hand, while the bias percentage for wind is high, the actual values are low. Therefore, this bias does not cause significant errors in the NET calculation, while the wind speed still has an important modifying effect.

For the calculated NET, the models performed well for almost all of the times examined (Figure 2). Averaged over the whole domain, there was some negative bias in almost all of the models. For the domain daytime when the maximums occur, the bias was under 10% for most of the models. The performance of the models was examined in detail with regards to simulating maximum heat stress by calculating the JJA average of the daily maximum temperature and NET (Figures 3 and 4), as well as the 95th percentile (Figures 5 and 6) for each model and ensembles, and comparing them with the values from JRA-55.

Figure 3 shows the spatial distribution of the average summer (JJA) maximum temperatures for JRA-55 and both ensembles, as well as the ensemble and model biases. The temperature distribution showed the highest values over the Indian Peninsula, northwest China, southeast China, and parts of Southeast Asia, specifically parts of Thailand, Cambodia, and Vietnam. The lowest values were observed over the Tibetan Plateau and the Himalayan region in general. Both ensembles (Figure 3a, b) and all the models individually reproduce this distribution fairly well. CMIP5_ens (Figure 3d) outperformed CMIP6_ens (Figure 3e). This might be because CMIP6_ens is forced by only one CGCM.

While the difference between ensembles was negligible for the majority of the domain, the most notable difference was the performance over the Indian Peninsula. Temperature bias over this area in CMIP6_ens was larger (up to 8°C) and more widespread (Figure 3e), while in CMIP5_ens (Figure 3d) it was limited to the northern part of Indian peninsula. CMIP5_ens outperformed all of the individual models, with the bias over the majority of the domain being relatively small (under 2°C, aside from bias over north of Indian Peninsula which reaches 5°C.

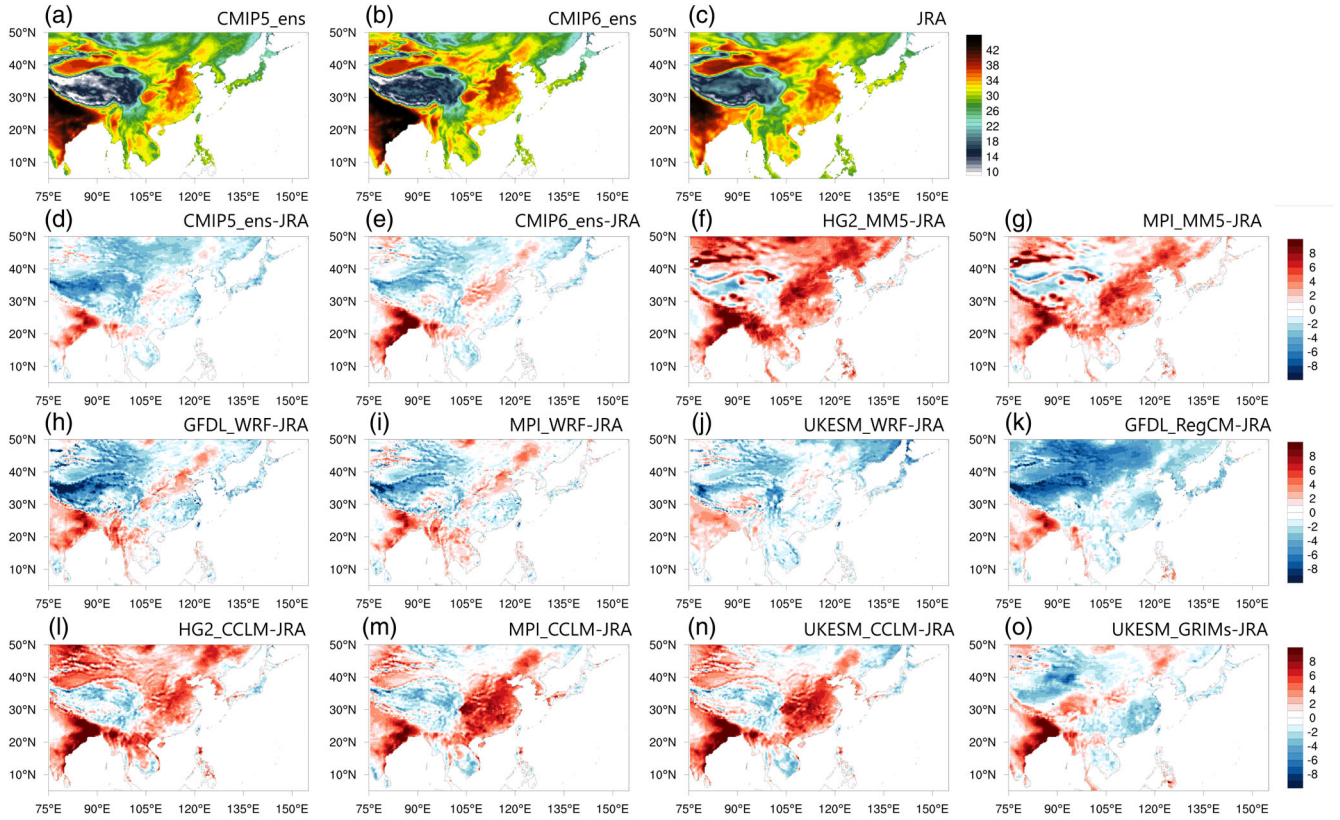

FIGURE 5 95th percentile of the temperature in °C for the summer (JJA) for the CMIP5_ens (a), CMIP6_ens (b), JRA (c), and the bias of both ensembles (d, e) and each model (f–o) [Colour figure can be viewed at wileyonlinelibrary.com]

Negative bias is largest over Tibetan Plateau, but is only around −3°C). The aforementioned bias over the Indian peninsula appears to be a systematic issue partially stemming from the global models, with chains using UKESM having more significant bias of up to 9°C in UKESM_CCLM and 8°C in UKESM_WRF (Figure 3j, n,o).

Figure 4 shows the spatial distribution of the average summer NET. The NET distribution mainly follows the temperature distribution, with the highest and lowest values over the Indian Peninsula and Tibetan Plateau, respectively. The difference is northwest China, where the NET values were not as high, likely due to humidity differences. Both CMIP5_ens and CMIP6_ens perform reasonably well with regards to the average maximum NET. The bias of the NET (Figure 4d,e) was smaller than the bias of the temperature (Figure 3d,e). Similar to temperature, CMIP5_ens outperformed CMIP6_ens, but the difference was smaller than the difference in the temperature simulations. Most individual models performed well for both NET and temperatures, with each model having the bias in different areas.

This analysis also showed that the large part of the negative bias % shown in Figures 1 and 2 originates from the negative bias over the Tibetan Plateau, where the temperatures are low. Therefore, even the relatively small negative bias of few °C translates to a relatively large bias percentage. In contrast, the positive bias over the northern end of the Indian Peninsula, where the temperatures are high, translates to a low bias percentage.

Figures 5 and 6 show the spatial distribution of the 95th percentile for temperature and NET, respectively. Similar to the average maximum temperatures and NETs, the ensembles outperformed the individual models. Interestingly, there was a much smaller difference in the performance of the CMIP5_ens and CMIP6_ens for the 95th percentile than for the average maximums. Both temperature and NET show systematic bias over the northeastern coast of the Indian Peninsula, which is larger in CMIP6_ens than in CMIP5_ens. There are larger domain areas with a negative bias for 95th percentile than for the average, particularly on the northern part of the domain (Figures 5d,e and 6d,e). Similar to the averages, the 95th percentile also has a smaller bias for the NET values than for the temperature values.

As a result, all of the models performed adequately for the purpose of the current research for both average summer maximum temperatures and NETs, as well as for simulating the value of the 95th percentile. Using as many models as possible for the simulations for the end of the 21st century is important because the uncertainties in these simulations are quite high. Furthermore, while the

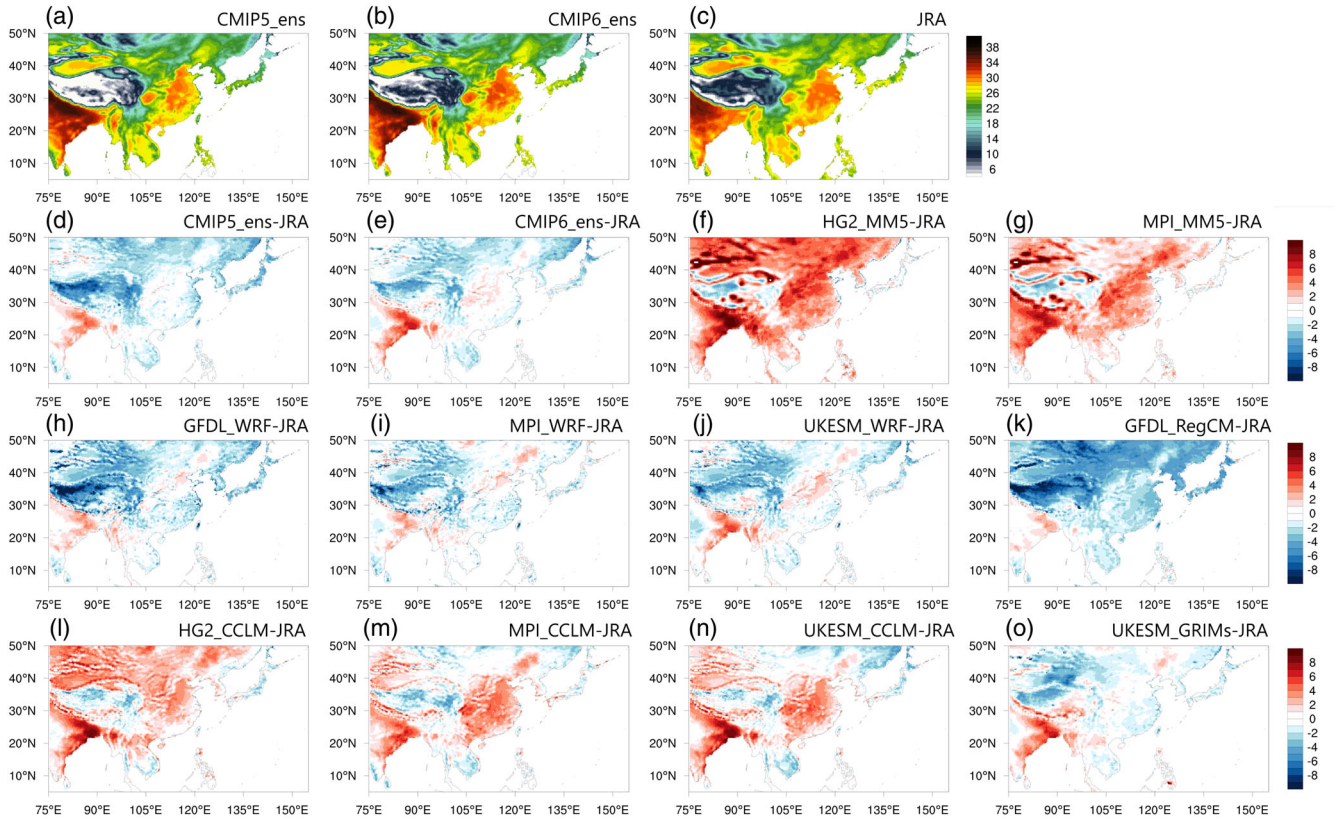

FIGURE 6 Same as Figure 5, but for NET [Colour figure can be viewed at wileyonlinelibrary.com]

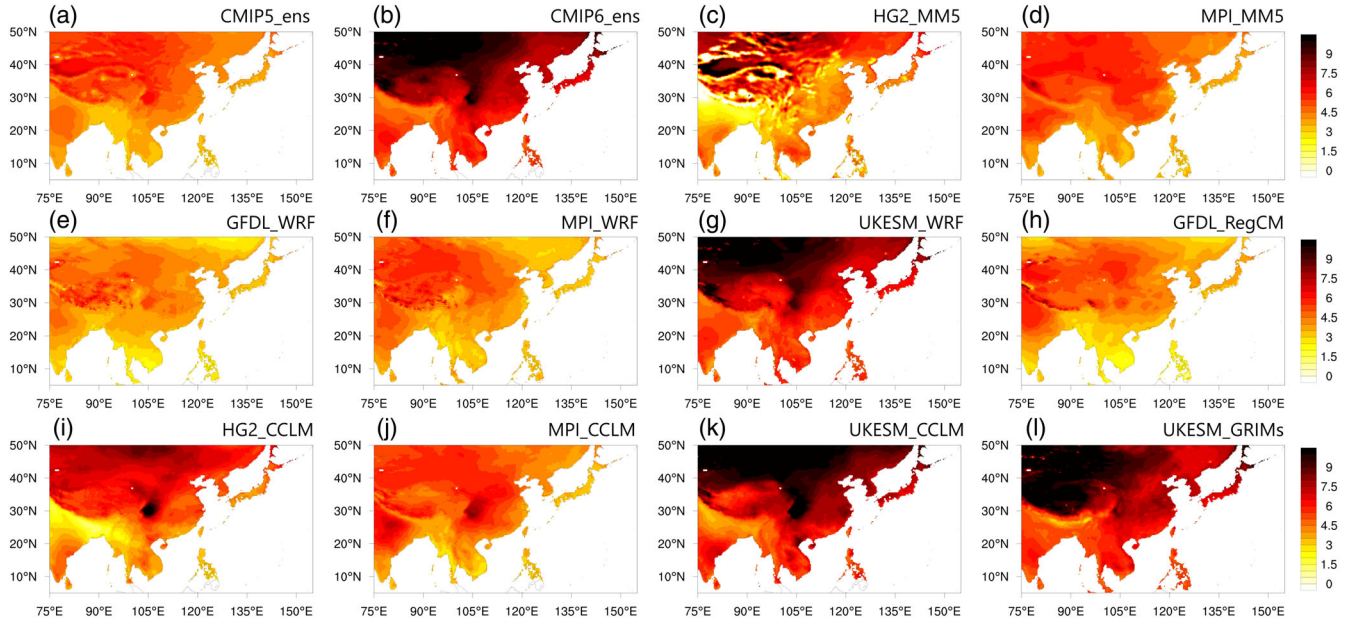

FIGURE 7 Change in the average summer (JJA) maximum temperature in °C for both ensembles (a, b) and all individual models (c–l) [Colour figure can be viewed at wileyonlinelibrary.com]

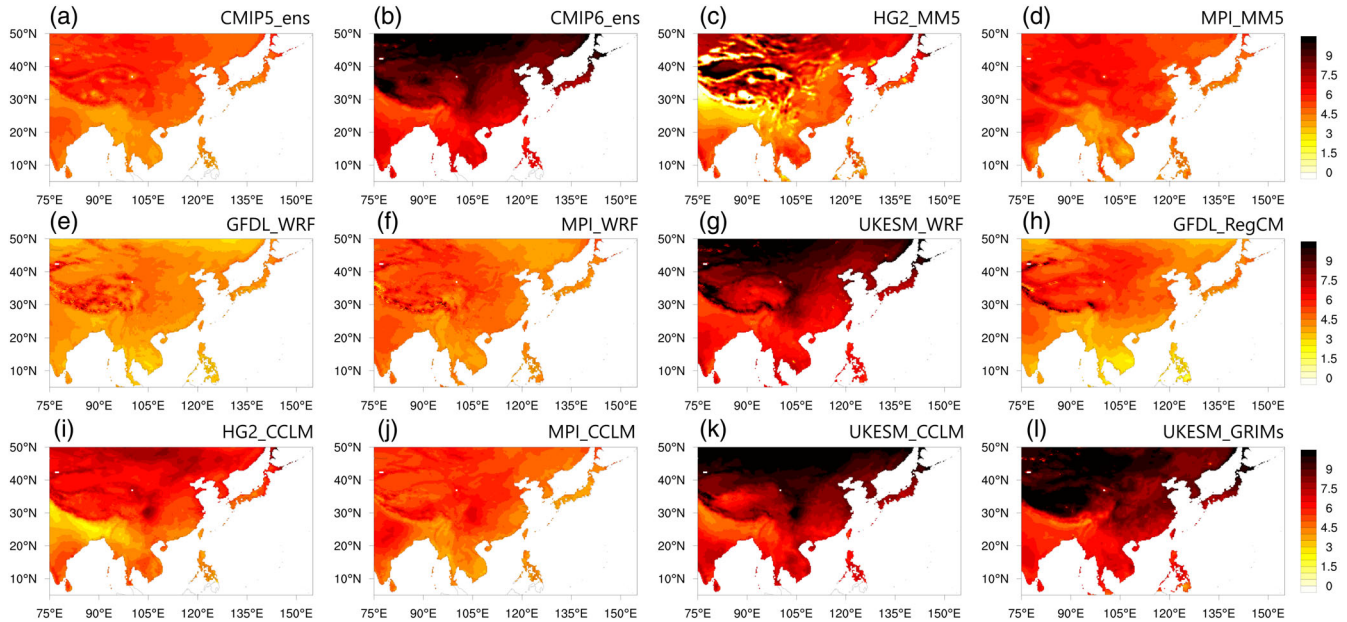

FIGURE 8 Same as Figure 7, but for NET [Colour figure can be viewed at wileyonlinelibrary.com]

domain-averaged bias for each 3-hourly value for NET is larger than for temperature, this appears to be the opposite of that in the seasonal averages of the daily maximums. This is due likely to two factors: the NET values are lower than the temperature, resulting in a higher bias percentage; and the maximums do not always occur at the same time.

After analysing the model performance regarding temperature and NET, it was decided to assess the impacts of climate change without bias correction for the temperature, humidity, and wind speed. A bias correction would have added additional uncertainties to the extremes and could have produced different results depending on the method used (e.g., Iizumi *et al.*, 2017). There is also a scarcity of studies on bias correction methods for wind and humidity.

3.2 | Future projections

Future projections have been made using two different scenarios. Unlike RCP scenarios, which only have the

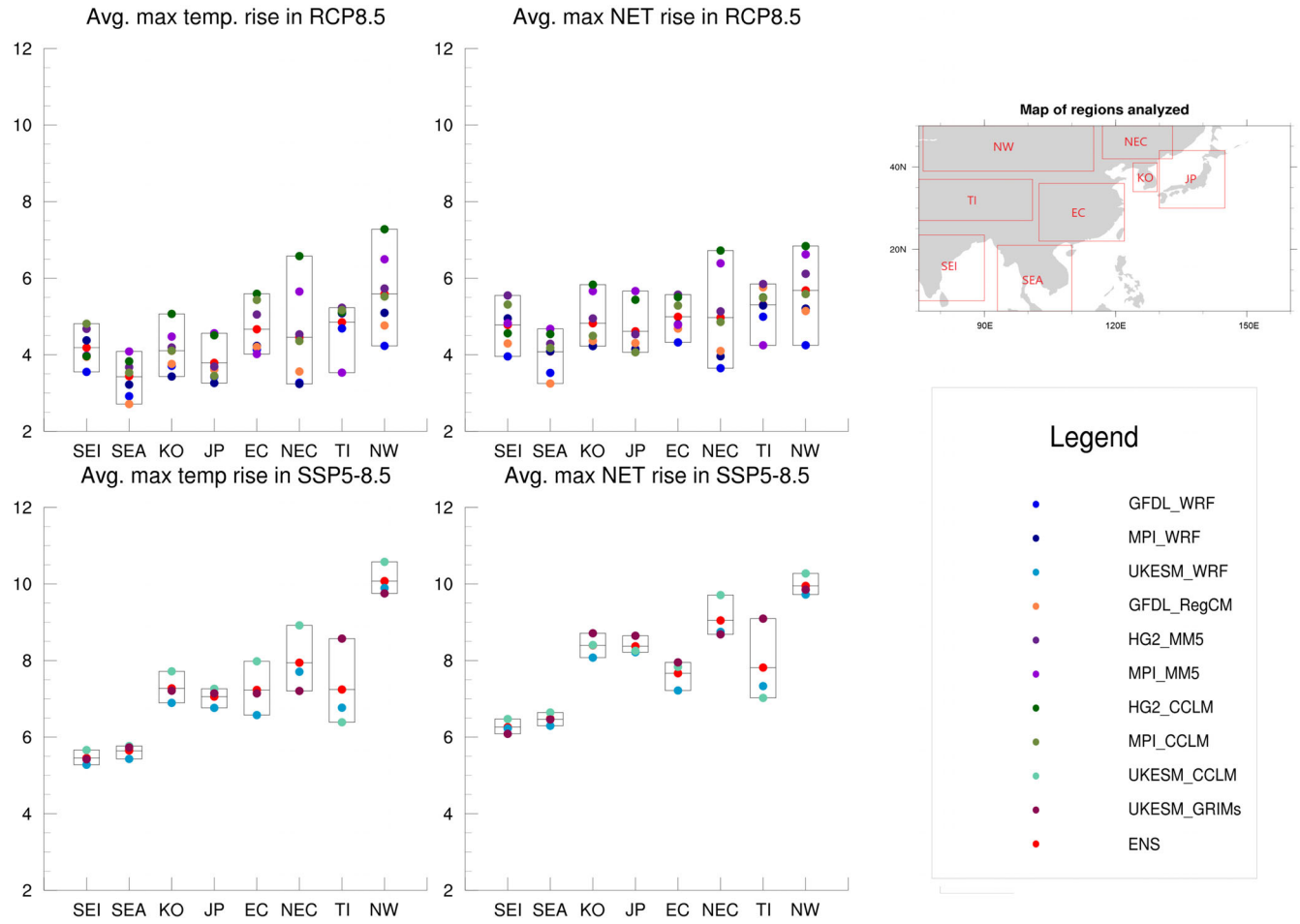

FIGURE 9 Map of regions and simulated regional changes in °C for temperature and NET for the end of the 21st century [Colour figure can be viewed at wileyonlinelibrary.com]

assumption of emissions, SSP scenarios consider population, economic growth, and other socioeconomic assumptions (O'Neill *et al.*, 2017). Both RCP8.5 and SSP5-8.5 are considered "worst-case scenarios." The CO_2 emissions at the end of the 21st century in the SSP5-8.5 are approximately 20% higher than in RCP8.5, resulting in more extreme warming (Riahi *et al.*, 2017).

Figures 7 and 8 show the average change in the seasonal average maximum temperatures and NETs for the ensembles and each model. The projected increase in temperature was higher in CMIP6_ens (up to 10°C, Figure 7b) than in CMIP5_ens (up to 7°C; Figure 7a). The pattern and the level of the change differed slightly from model to model. In particular, the level of change appeared to depend more on the global model used than the RCM, with the GFDL-ESM2M-based model chains showing the lowest (Figure 7e,h), and the HadGEM2-AO based models showing the highest temperature change (Figure 7c,i).

In SSP5-8.5 based CMIP6_ens, one global model was used. Hence, the spread between models is smaller than in the RCP8.5 based CMIP5_ens. Taking that into consideration, there were similarities between the temperature change patterns of CMIP5_ens and CMIP6_ens. Both scenarios project a higher level of warming in the higher latitudes (Figure 7a,b). The smallest changes were projected over the northern end of the Indian Peninsula under the Himalayan mountains. In the RCP8.5, a lower change was also projected over Bangladesh and Myanmar. On the other hand, these areas already experience extreme heat during the summer in the current climate. Therefore, even with the change being smaller than in the rest of the domain, it might significantly affect human lives in this densely populated area. Regarding NET, the change patterns closely followed the temperature pattern, with the change being greater for the NET than for the temperature (Figure 8). Similarly, as with temperature, the projected change was several degrees C higher in the SSP5-8.5 than in the RCP8.5. The projected change in heat stress was higher than the temperature, highlighting the importance of considering other factors when researching future climate projections rather than just

temperature and precipitation. This high increase in heat stress could pose a significant danger to the ecosystems and the human lives in all areas affected by it.

Figure 9 shows the projected temperature and NET rise over the different domains for the RCP8.5 (CMIP5 models) and SSP5-8.5 (CMIP6 models) scenarios. The change in temperature is projected to be highest in the northwest part of the domain (northwest China and Mongolia region, NW) in both RCP8.5 (4.2–7.3°C) and SSP5-8.5 scenarios (9.7–10.6°C). While on average the rise in NET is projected to be higher than the rise in temperature for all models (by around 0.5°C on average in RCP8.5 and around 1°C on average in SSP5-8.5), some of the models predict different scenarios for some of the regions (e.g., HG2_CCLM predicts higher temperature than NET rise for NW in RCP8.5 scenario). Additionally,

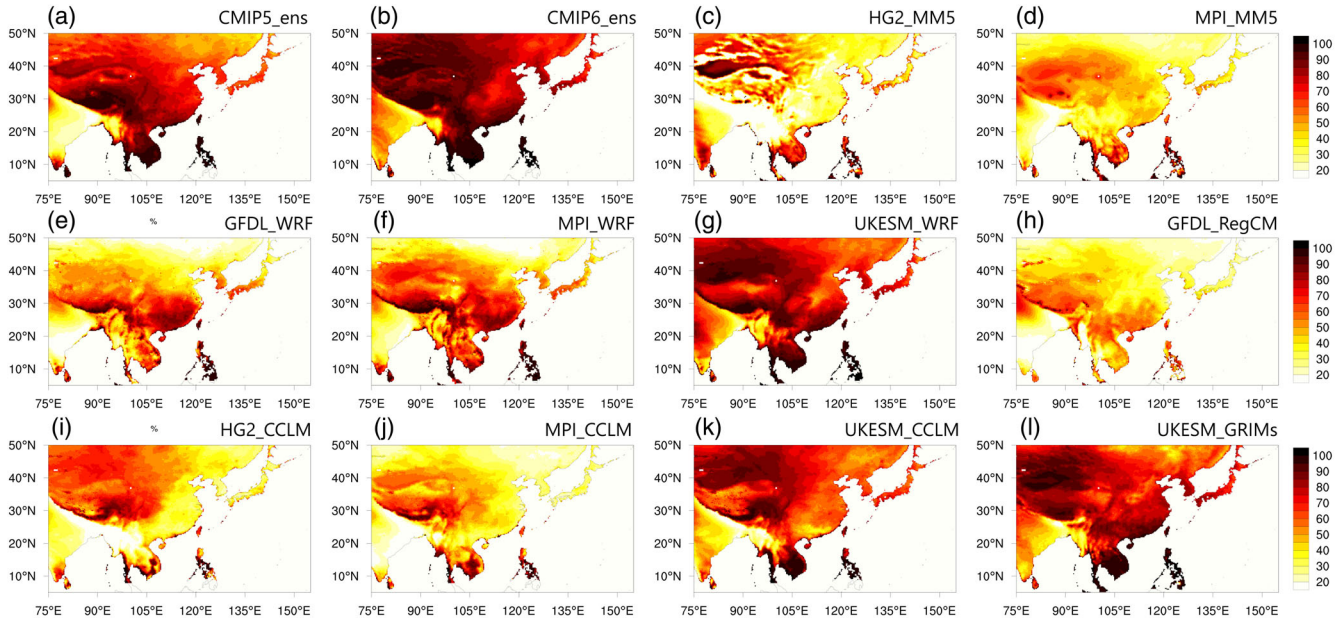

FIGURE 10 Percentage of the daily maximum temperatures over the historical 95th percentile at the end of the 21st century for both ensembles (a, b) and all individual models (c–l) [Colour figure can be viewed at wileyonlinelibrary.com]

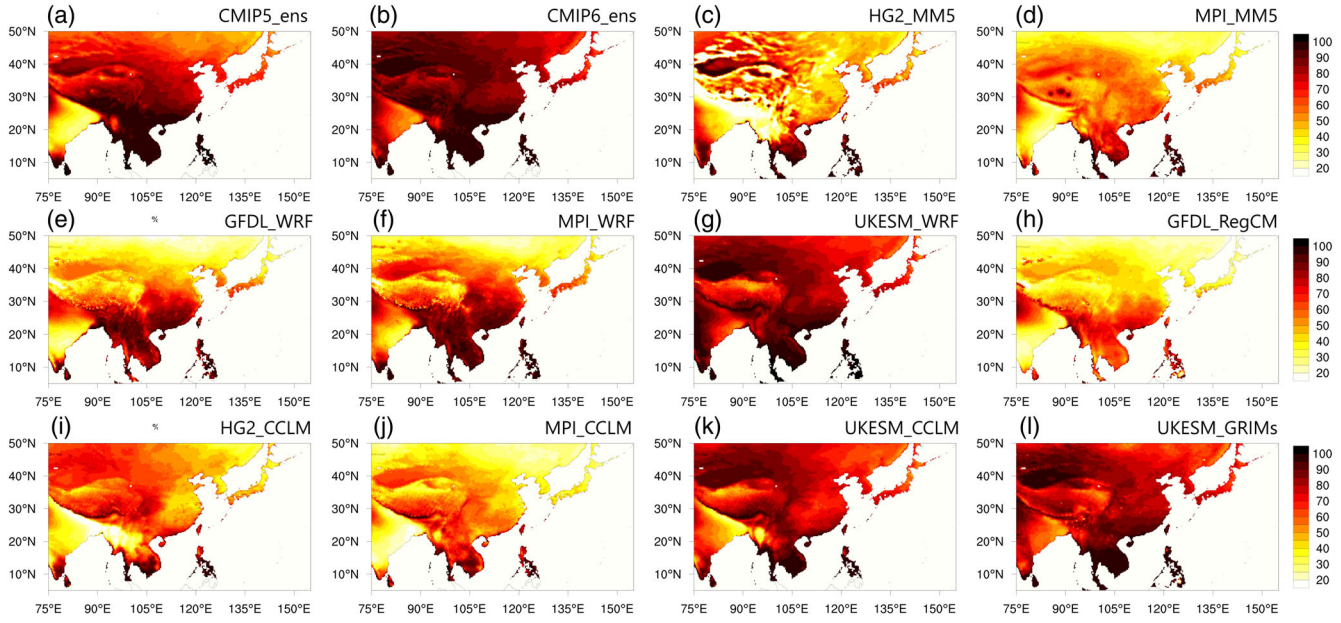

FIGURE 11 Same as Figure 10, just for the NET [Colour figure can be viewed at wileyonlinelibrary.com]

the smallest rise is projected in the Southeast Asia (SEA) in the RCP8.5 (2.7–4.1°C), and southeast India (SEI) in SSP5-8.5 scenario (4.0–5.3°C). Model spread for most regions is much larger in RCP8.5 scenario, likely due to the fact that more models have been used, with the largest spread being over northeast China (NEC) and NW in RCP8.5 scenario and over Tibetan Plateau (TI) in SSP5-8.5 scenario. The differences between increase in NET and temperature are the highest in Korean Peninsula (KO) and Japan (JP), with increase in NET being 0.7/0.8°C in RCP8.5 and 1.1/1.3°C in SSP5-8.5 higher than increase in temperature for KO and JP, respectively. NW is the only region for which projected change in NET and temperature are approximately the same on average. This is most likely because that region is less humid in general, and therefore the changes in NET follow closely the changes in temperature.

Finally, the important factor in heat stress change is not just the change in the average summer values but the frequency of the extremes. Previous research showed that extreme events are projected to increase in the future (Li *et al*., 2018). Therefore, this study examined how frequent the values over the historical 95th percentile are projected to be at the end of the 21st century. Figures 10 and 11 show the results for the temperature and the NET, respectively. The figures show the percentage of the summer days with the temperature over the historical 95th percentile value for each grid point. The changes in the percentage of days over 95th percentile appeared to be inflated in the ensembles (Figures 10a,b and 11a,b) compared to the results from each model (Figures 10c–l and 11c–l). The reason might be that the models predict the highest increases in slightly different parts of the domain, such as chains including HadGEM2-AO predicting a larger increase in the northwest part of the domain (Figure 10c,i), while the MPI-ESM-LR and GFDL-ESM2M-based chains predict larger increases in the middle of the domain (Figure 10d,e,f,j). Therefore, the analysis focused mainly on the individual models and the similarities and differences between them. All the models agree on the 95th percentile value becoming a common occurrence (>30% in RCP8.5 and >50% in SSP5-8.5 for most of the domain). In some areas already impacted by high heat stress, such as Thailand, Cambodia, and SE China, the 95th percentile values are predicted to become the standard (>80% of days) in the SSP5-8.5 scenario. This change is even higher for the NET, meaning that the combined changes in temperature, humidity, and wind could make the experience of heat even worse (Figure 11). Even in the RCP8.5, large parts of the domain are projected to experience NETs over the current 95th percentile on approximately 50% of the days in summer. The simulations with the SSP5-8.5 predict that these values could become a daily or almost daily occurrence in large areas of the domain, mainly in Southeast Asia and parts of the Indian Peninsula.

Overall, while the average change in the temperature and NET values themselves is larger in the northern part of the domain, the changes in the frequency are more significant in the southern end of the domain, because this part of the domain already struggles with heatwaves in the current climate. Moreover, increasing the frequency of them would adversely impact large populations living in that area.

While very few regions are experiencing NETs over 33°C in the current climate (Figure 6a–c), these areas are projected to become much wider and experience this type of heat stress much more often in a future climate (Figures 8 and 11). This could pose a large problem because human adaptability has limits. The human body needs to maintain its normal temperature. Temperature regulation becomes impossible when the combination of heat and humidity reaches the point at which there is no way for the heat to be dissipated. This can lead to heatstroke, and ultimately, death if exposed to these conditions for several hours. This study suggests that the projected change in NET could be over the limit of human adaptability in certain parts of the East Asia domain.

4 | CONCLUSIONS AND DISCUSSION

Although it is expected that global warming will induce changes in climate worldwide, regional aspects can be disproportionate and nonlinear with the global temperature rise. Some areas might experience a much greater rise in temperature than the overall global level of warming, bringing unwanted consequences for ecosystems and humans. The temporal and spatial patterns of climate change on a regional scale remain relatively uncertain (e.g., Harrington *et al*., 2018). Therefore, it is important to quantify the possible effects to allow the local mitigation efforts.

In this study, the simulations from four CGCMs downscaled with five different RCMs to form a total of 10 CGCM-RCM chains were used to assess the regional impact of global warming by the end of the 21st century. JRA-55 reanalysis data were used to evaluate the performance of the models. The performance of the models and the ensembles was first evaluated for each variable used to calculate the NET separately. All variables used to calculate the NET, that is, temperature, humidity, and wind, were sufficiently simulated in all of the models on their own, as well as the NET itself, with temperature and

NET having smaller bias than humidity and wind. Therefore, the historical simulations of all of the models reproduced the current climate reasonably, with the ensembles outperforming the individual models, particularly CMIP5_ens. Furthermore, the model overview from this study can be a useful starting point for future research on more specific areas because it shows that some models perform better in some areas than others, such as the HG2_MM5 chain having a positive bias over the north and west parts of the domain while performing well over Japan (Figure 4f) and the MPI_MM5 chain performing well over Southeast Asia (Figure 4g).

The simulations for the end of the 21st century with RCP8.5 and SSP5-8.5 both showed overall increases in temperature, which are consistent with previous studies, as well as an increase in NET. The projected increase in NET was higher than the increase in temperature itself in most of the regions, leading to the worse experience of heat stress (Figure 9), with the models having largest spread over NW and NEC in RCP8.5, and over TI in SSP5-8.5 scenario for both temperature and NET. In addition, this study showed that while the increase in temperature and NET itself was higher over the northern part of the domain, the increase in the frequency of the extreme values was higher over some of the already vulnerable parts of the domain, such as Southeast Asia, and parts of the Tibetan Plateau. The magnitude of the change, that is, the average rise in temperature and NET was mostly dependent on the choice of the scenario. The overall higher emissions in SSP5-8.5 translate into higher projected temperatures and NETs overall. The details of the warming patterns, on the other hand, were more dependent on the CGCM and RCM choices, rather than the scenario choice.

Humans have a certain threshold of tolerance to high temperatures and humidity—the absolute limit of human adaptability is the wet bulb temperature of 35°C. While the human limit for NET is not exactly defined, even in the current climate the summer heatwaves are often deadly. The findings of this study, that is, those extreme temperatures becoming a very common occurrence (Figures 10 and 11), along with rise of NET being higher than rise of temperature itself (Figures 7 and 8) support Im *et al.* (2017), who predicted that certain densely populated areas would exceed the threshold of human adaptability by the end of the 21st century. This could have an immense impact on the populations living in those areas, effectively making them more difficult, if not impossible, to live in and displacing millions of people. Therefore, it is a high priority to limit the climate change as much as possible, trough the global cooperation on lowering the greenhouse emissions. While the effects of the climate change can have much higher impacts locally, mitigating the climate change also requires global action. Additionally, knowing the possible local impacts of climate change allows for some adaptations—for example, adapting food production to the cultures that will thrive in hotter environments, adjusting planting periods to provide higher yields, and other agricultural adjustments (Aryal *et al.*, 2020). Furthermore, knowing that some areas are likely to become uninhabitable in the future would allow more time for the slower, gradual movement of the people from those areas.

Present study has a potential limitation in the fact that urban parameterization has not been used in the model simulations, and therefore the effects of heat stress changes in megacities are not taken into account. Urban parameterization is a very important factor in the very high-resolution models, where the effects of heat islands can be shown, but also has impact on somewhat coarser resolution scale. However, Katzfey *et al.* (2020) showed that the effects of urban parameterization on maximum temperatures are small and not statistically significant at 50 km resolution in Asian region. Huszar *et al.* (2014) showed the similar thing using RegCM that the impact is important when simulating nighttime temperatures, but less so when simulating daytime temperatures. As the current study focuses on the general changes in the maximum daytime heat stress over the East Asia domain, rather than megacities and their surroundings, applying urban parameterization likely would not change results, but it is something to be taken into account when researching heat stress over the smaller areas, especially over densely populated megacities (e.g., Argüeso *et al.*, 2015; Yang *et al.*, 2016; Takane *et al.*, 2020).

ACKNOWLEDGEMENT

This work was funded by the Korea Meteorological Administration Research and Development Program under Grant KMI2020-01411.

AUTHOR CONTRIBUTIONS

A. Juzbašić: Conceptualization; formal analysis; investigation; writing – original draft; writing – review and editing. **J. B. Ahn:** Conceptualization; funding acquisition; investigation; supervision. **D. H. Cha:** Data curation; investigation. **E. C. Chang:** Data curation; investigation. **S. K. Min:** Data curation; investigation.

DATA AVAILABILITY STATEMENT

Data (model simulations) used in this study are available upon reasonable request from the authors, and will be publicly available at https://esg-dn1.nsc.liu.se/search/cordex/ in the future. JRA-55 dataset is publicly available: https://doi.org/10.2151/jmsj.2015-001.

ORCID

Ana Juzbašić https://orcid.org/0000-0002-3820-790X
Joong-Bae Ahn https://orcid.org/0000-0001-6958-2801
Dong-Hyun Cha https://orcid.org/0000-0001-5053-6741
Eun-Chul Chang https://orcid.org/0000-0002-5784-447X
Seung-Ki Min https://orcid.org/0000-0002-6749-010X

REFERENCES

Ahn, J., Jo, S., Suh, M., Cha, D.H., Lee, D.K., Hong, S.Y., Min, S.K., Park, S.C., Kang, S.H. and Shim, K.M. (2016) Changes of precipitation extremes over South Korea projected by the 5 RCMs under RCP scenarios. *Asia-Pacific Journal of Atmospheric Sciences*, 52, 223–236. https://doi.org/10.1007/s13143-016-0021-0.

Argüeso, D., Evans, J.P., Pitman, A.J. and Di Luca, A. (2015) Effects of city expansion on heat stress under climate change conditions. *PLoS One*, 10(2), e0117066. https://doi.org/10.1371/journal.pone.0117066.

Aryal, J.P., Sapkota, T.B., Khurana, R., Khatri-Chhetri, A., Rahut, d.b. and Jat, M.L. (2020) Climate change and agriculture in South Asia: adaptation options in smallholder production systems. *Environment, Development and Sustainability*, 22, 5045–5075. https://doi.org/10.1007/s10668-019-00414-4.

Blazejczyk, K., Epstein, Y., Jendritzky, G., Staiger, H. and Tinz, B. (2011) Comparison of UTCI to selected thermal indices. *International Journal of Biometeorology*, 56, 515–535. https://doi.org/10.1007/s00484-011-0453-2.

Bröde, P., Fiala, D., Błażejczyk, K., Holmér, I., Jendritzky, G., Kampmann, B., Tinz, B. and Havenith, G. (2012) Deriving the operational procedure for the universal thermal climate index (UTCI). *International Journal of Biometeorology*, 56, 481–494. https://doi.org/10.1007/s00484-011-0454-1.

Casanueva, A., Kotlarski, S., Herrera, S., Fischer, A.M., Kjellstrom, T. and Schwierz, C. (2019) Climate projections of a multivariate heat stress index: the role of downscaling and bias correction. *Geoscience Model Development*, 12, 3419–3438. https://doi.org/10.5194/gmd-12-3419-2019.

Ciarlo, J.M., Coppola, E., Fantini, A., Giorgi, F., Gao, X.J., Tong, Y., Glazer, R.H., Alavez, J.A.T., Sines,T., Pichelli,E., Raffaele, F., Das, S., Bukovsky, M., Ashfaq, M., Im, E-S., Nguyen-Xuan, T., Teichmann, T., Remedio, A., Remke, T., Bülow, K., Weber, T., Buntemeyer, L., Sieck, k., Rechid, D. and Jacob, D. (2021) A new spatially distributed added value index for regional climate models: the EURO-CORDEX and the CORDEX-CORE highest resolution ensembles. *Climatte Dynamics*, 57, 1403–1424. https://doi.org/10.1007/s00382-020-05400-5.

Diffenbaugh, N.S., Pal, J.S., Giorgi, F. and Gao, X. (2007) Heat stress intensification in the Mediterranean climate change hotspot. *Geophysical Research Letters*, 34, L11706. https://doi.org/10.1029/2007GL030000.

Doms, G. and Baldauf, M. (2013) *A Description of the Nonhydrostatic Regional COSMO-Model, Part I: Dynamics and Numerics*. DWD (Deutscher Wetterdienst), Offenbach, Germany. https://doi.org/10.5676/dwd_pub/nwv/cosmo-doc_5.05_i.

Dunne, J.P., John, J.G., Adcroft, A.J., Griffies, S.M., Hallberg, R.W., Shevliakova, E., Stouffer, R.J., Cooke, W., Dunne, K.A., Harrison, M.J., Krasting, J.P., Malyshev, S.L., Milly, P. C. D., Phillipps, P.J., Sentman, L.T., Samuels, B.L., Spelman, M.J., Winton, M., Wittenberg, A.T. and Zadeh, N. (2012) GFDL's ESM2 global coupled climate–carbon earth system models. Part I: physical formulation and baseline simulation characteristics. *Journal of Climate*, 25, 6646–6665. https://doi.org/10.1175/JCLI-D-11-00560.1.

Giorgetta, M.A., Jungclaus, J., Reick, C.H., Legutke, S., Bader, J., Böttinger, M., Brovkin, V., Crueger, T., Esch, M., Fieg, K., Glushak, K., Gayler, V., Haak, H., Hollweg, H.D., Ilyina, T., Kinne, S., Kornblueh, L., Matei, D., Mauritsen, T., Mikolajewicz, U., Mueller, W., Notz, D., Pithan, F., Raddatz, T., Rast, S., Redler, R., Roeckner, E., Schmidt, H., Schnur, R., Segschneider, J., Six, K.D., Stockhause, M., Timmreck, C., Wegner, J., Widmann, H., Wieners, K.H., Claussen, M., Marotzke, J. and Stevens, B. (2013) Climate and carbon cycle changes from 1850 to 2100 in MPI-ESM simulations for the Coupled Model Intercomparison Project phase 5. *Journal of Advances in Modeling Earth Systems*, 5, 572–597. https://doi.org/10.1002/jame.20038.

Giorgi, F., Coppola, E., Solomon, F., Mariotti, L., Sylla, M.B., Bi, X., Elguindi, N., Diro, G. T., Nair, V., Giuliani, G., Turuncoglu, U. U., Cozzini, S., Güttler, I., O'Brien, T.A., Tawfik, A.B., Shalaby, A., Zakey, A.S., Steiner, A.L., Stordal, F., Sloan, L.C. and Brankovic, C. (2012) RegCM4: model description and preliminary tests over multiple CORDEX domains. *Climate Research*, 52, 7029. https://doi.org/10.3354/cr01018.

Grell, G.A., Dudhia, J. and Stauffer, D.R. (1994) *A description of the Fifth-Generation Penn State/NCAR mesoscale model (MM5)*. Boulder, CO: NCAR. Technical note: NCAR/TN-398+STR. https://doi.org/10.5065/D60Z716B.

Harrington, L.J., Frame, D., King, A.D. and Otto, F.E.L. (2018) How uneven are changes to impact-relevant climate hazards in a 1.5°C world and beyond? *Geophysical Research Letters*, 45, 6672–6680. https://doi.org/10.1029/2018GL078888.

Hong, S.-Y., Park, H., Cheong, H.-B., Kim, J.-E.E., Koo, M.-S., Jang, J., Ham, S., Hwang, S.-O. Park, B.-K., Chang, E.-C. and Li, H. (2013) The global/regional integrated model system (GRIMs). *Asia-Pacific Journal of Atmospheric Sciences*, 49, 219–243. https://doi.org/10.1007/s13143-013-0023-0.

Höppe, P. (1999) The physiological equivalent temperature—a universal index for the biometeorological assessment of the thermal environment. *International Journal of Biometeorology*, 43, 71–75. https://doi.org/10.1007/s004840050118.

Huszar, P., Halenka, T., Belda, M., Zak, M., Sindelarova, K. and Miksovsky, J. (2014) Regional climate model assessment of the urban land-surface forcing over central Europe. *Atmospheric Chemistry and Physics*, 14, 12393–12413. https://doi.org/10.5194/acp-14-12393-2014.

Iizumi, T., Takikawa, H., Hirabayashi, Y., Hanasaki, N. and Nishimori, M. (2017) Contributions of different bias-correction methods and reference meteorological forcing data sets to uncertainty in projected temperature and precipitation extremes. *Journal of Geophysical Research: Atmospheres*, 122, 7800–7819. https://doi.org/10.1002/2017JD026613.

Im, E.S., Pal, J.S. and Eltahir, E.A.B. (2017) Deadly heat waves projected in the densely populated agricultural regions of South Asia. *Science Advances*, 3(8), e1603322. https://doi.org/10.1126/sciadv.1603322.

IPCC. (2007) *Climate Change 2007: Synthesis Report. Contribution of Working Groups I, II and III to the Fourth Assessment Report of the Intergovernmental Panel on Climate Change*. Cambridge: IPCC.

IPCC. (2014) *Climate Change 2014: Synthesis Report. Contribution of Working Groups I, II and III to the Fifth Assessment Report of the Intergovernmental Panel on Climate Change*. Cambridge: IPCC.

Japan Meteorological Agency. (2013) *JRA-55: Japanese 55-year Reanalysis, Daily 3-Hourly and 6-Hourly Data*. Research Data Archive at the National Center for Atmospheric Research, Computational and Information Systems Laboratory. https://doi.org/10.5065/D6HH6H41.

Jo, S., Ahn, J.B., Cha, D.H., Min, S.K., Suh, M.S., Byun, Y.H. and Kim, J.U. (2019) The Köppen–Trewartha climate-type changes over the CORDEX-East Asia phase 2 domain under 2 and 3°C global warming. *Geophysical Research Letters*, 46, 14030–14041. https://doi.org/10.1029/2019GL085452.

Jo, S.R., Shim, K.M., Hur, J.N., Kim, Y.S. and Ahn, J.B. (2020) Future changes of agro-climate and heat extremes over S. Korea at 2 and 3°C global warming levels with CORDEX-EA phase 2 projection. *Atmosphere*, 11, 1336. doi:10.3390/atmos11121336

Jones, T.S., Liang, A.P., Kilbourne, E.M., Griffin, M.R., Patriarca, P. A., Fite Wassilak, S.G., Griffin, M.R., Patriarca, P.A. Fite Wassilak, S.G., Mullan, R.J., Herrick, R.F., Donnell, H.D. Jr, Choi, K. and Thacker, S.B. (1982) Morbidity and mortality associated with the July 1980 heat wave in St. Louis and Kansas City, MO. *Journal of the American Medical Association*, 247, 3327–3331.

Kalkstein, L.S. and Davis, R.E. (1985) The impact of winter weather on human mortality for environmental impact assessment. In: *Proceedings of the 7th Conference of Biometeorology and Aerobiology, Scottsdale, AZ, 21–24 May 1985*, pp. 334–336. American Meteorological Society. Boston, MA.

Katzfey, J., Schlünzen, H., Hoffmann, P. and Thatcher, M. (2020) How an urban parameterization affects a high-resolution global climate simulation. *Quarterly Journal of the Royal Meteorological Society*, 146, 3808–3829. doi:10.1002/qj.3874

Kobayashi, S., Ota, Y., Harada, Y., Ebita, A., Moriya, M., Onoda, H., Onogi, K., Kamahori, H., Kobayashi, C., Endo, H., Miyaoka, K. and Takahashi, K. (2015) The JRA-55 reanalysis: general specifications and basic characteristics. *Journal of the Meteorological Society of Japan*, 93, 5–48. https://doi.org/10.2151/jmsj.2015-001.

Lee, J.W. and Hong, S.Y. (2014) Potential for added value to downscaled climate extremes over Korea by increased resolution of a regional climate model. *Theoretical and Applied Climatology*, 117, 667–677. https://doi.org/10.1007/s00704-013-1034-6.

Lee, S.M. and Min, S.K. (2018) Heat stress changes over East Asia under 1.5° and 2.0°C global warming targets. *Journal of Climate*, 31(7), 2819–2831. https://doi.org/10.1175/JCLI-D-17-0449.1.

Li, D.H., Zou, L.W. and Zhou, T.J. (2018) Extreme climate event changes in China in the 1.5°C and 2°C warmer climates: results from statistical and dynamical downscaling. *Journal of Geophysical Research: Atmospheres*, 123, 10196–10211. doi:10.1029/2018JD028835

Li, p.W. and Chan, S.T. (2000) Application of a weather stress index for alerting the public to stressful weather in Hong Kong. *Meteorological Applications*, 7, 369–375. https://doi.org/10.1017/S1350482700001602.

Martin, G.M., Bellouin, N., Collins, W.J., Culverwell, I.D., Halloran, p.R., Hardiman, S.C., Hinton, T.J., Jones, C.D., McDonald, R.E., McLaren, A.J., O'Connor, F.M., Roberts, M.J., Rodriguez, J.M., Woodward, S., Best, M.J., Brooks, M.E., Brown, A.R., Butchart, N., Dearden, C., Derbyshire, S.H., Dharssi, I., Doutriaux-Boucher, M., Edwards, J.M., Falloon, P. D., Gedney, N., Gray, L.J., Hewitt, H.T., Hobson, M., Huddleston, M.R., Hughes, J., Ineson, S., Ingram, W.J., James, P.M., Johns, T.C., Johnson, C.E., Jones, A., Jones, C.P., Joshi, M.M., Keen, A.B., Liddicoat, S., Lock, A.P., Maidens, A.V., Manners, J.C., Milton, S.F., Rae, J.G.L., Ridley, J.K., Sellar, A., Senior, C.A., Totterdell, I.J., Verhoef, A., Vidale, P.L. and Wiltshire, A. (2011) The HadGEM2 family of Met Office unified model climate configurations. *Geoscientific Model Development*, 4, 723–757. https://doi.org/10.5194/gmd-4-723-2011.

Missenard, A. (1937) Warmth and comfort. *Journal of the Institution of Heating and Ventilating Engineers*, 4, 602–606.

Ngo-Duc, T., Tangang, F.T., Santisirisomboon, J., Cruz, F., Trinh-Tuan, L., Nguyen-Xuan, T., Phan-van, T., Juneng, L., Narisma, G., Singhruck, P., Gunawan, D. and Aldrian, E. (2016) Performance evaluation of RegCM4 in simulating extreme rainfall and temperature indices over the CORDEX-Southeast Asia region. *International Journal of Climatology*, 37, 1634–1647. https://doi.org/10.1002/joc.4803.

O'Neill, B.C., Kriegler, E., Ebi, K.L., Kemp-Benedict, E., Riahi, K., Rothman, D.S., van Ruijven, B.J., van Vuuren, D.P., Birkmann, J., Kok, K., Levy, M. and Solecki, W. (2017) The roads ahead: narratives for shared socioeconomic pathways describing world futures in the 21st century. *Global Environmental Change*, 42, 169–180. https://doi.org/10.1016/j.gloenvcha.2015.01.004.

Oh, S.-G., Park, J.-H., Lee, S.-H. and Suh, M.-S. (2014) Assessment of the RegCM4 over East Asia and future precipitation change adapted to the RCP scenarios. *Journal of Geophysical Research: Atmospheres*, 119, 2913–2927. https://doi.org/10.1002/2013JD020693.

Okada, M. and Kusaka, H. (2013) Proposal of a new equation to estimate globe temperature in an urban park environment. *Journal of Agricultureal Meteorology*, 69(1), 23–32. https://doi.org/10.2480/agrmet.69.1.4.

Park, C. and Min, S. (2019) Multi-RCM near-term projections of summer climate extremes over East Asia. *Climate Dynamics*, 52, 4937–4952. https://doi.org/10.1007/s00382-018-4425-7.

Park, C., Min, S., Lee, D.H., Cha, D.H., Suh, M.S., Kang, H.S., Hong, S.Y., Lee, D.K., Baek, H.J., Boo K.O. and Kwon, W.T. (2016) Evaluation of multiple regional climate models for summer climate extremes over East Asia. *Climate Dynamics*, 46, 2469–2486. https://doi.org/10.1007/s00382-015-2713-z.

Powers, J.G., Klemp, J.B., Skamarock, W.C., Davis, C.A., Dudhia, J., Gill, D.O., Coen, J.L., Gochis, D.J., Ahmadov, R., Peckham, S. E., Grell, G.A., Michalakes, J., Trahan, S., Benjamin, S.G., Alexander, C.R., Dimego, G.J., Wang, W., Schwartz, C.S., Romine, G.S., Liu, Z., Snyder, C., Chen, F., Barlage, M.J., Yu, W. and Duda, M.G. (2017) The weather research and forecasting model: overview, system efforts, and future directions. *Bulletin of American Meteorological Society*, 98(8), 1717–1737. https://doi.org/10.1175/BAMS-D-15-00308.1.

Prajapat, D.K., Lodha, J. and Choudhary, M. (2019) A spatiotemporal analysis of Indian warming target using CORDEX-SA experiment data. *Theoretical and Applied Climatology*, 139, 447–459. https://doi.org/10.1007/s00704-019-02978-7.

Riahi, K., van Vuuren, D.P., Kriegler, E., Edmonds, J., O'Neill, B.C., Fujimori, S., Bauer, N., Calvin, K., Dellink, R., Fricko, O.,

Lutz, W., Popp, A., Cuaresma, J.C., KC, S., Leimbach, M., Jiang, L., Kram, T., Rao, S., Emmerling, J., Ebi, K., Hasegawa, T., Havlik, P., Humpenöder, F., da Silva, L.A., Smith, S., Stehfest, E., Bosetti, V., Eom, J., Gernaat, D., Masui, T., Rogelj, J., Strefler, J., Drouet, L., Krey, V., Luderer, G., Harmsen, M., Takahashi, K., Baumstark, L., Doelman, J.C., Kainuma, M., Klimont, Z., Marangoni, G., Lotze-Campen, H., Obersteiner, M., Tabeau, A. and Tavoni, M. (2017) The shared socioeconomic pathways and their energy, land use, and greenhouse gas emissions implications: an overview. *Global Environmental Change*, 42, 153–168. https://doi.org/10.1016/j.gloenvcha.2016.05.009.

Ritchie, H. and Roser, M. (2020) CO_2 and greenhouse gas emissions. Available at: OurWorldInData.org.

Sellar, A.A., Jones, C.G., Mulcahy, J.P., Tang, Y., Yool, A. and Wiltshire, A. (2019) UKESM1: description and evaluation of the U.K. Earth system model. *Journal of Advances in Modeling Earth Systems*, 11(12), 4513–4558. https://doi.org/10.1029/2019MS001739.

Steadman, R.G. (1984) A universal scale of apparent temperature. *Journal of Applied Meteorology*, 23(12), 1674–1687.

Stull, R. (2011) Wet-bulb temperature from relative humidity and air temperature. *Journal of Applied Meteorology and Climatology*, 50, 2267–2269. https://doi.org/10.1175/JAMC-D-11-0143.1.

Suzuki-Parker, A. and Kusaka, H. (2016) Future projections of labor hours based on WBGT for Tokyo and Osaka, Japan, using multi-period ensemble dynamical downscale simulations. *International Journal of Biometeorology*, 60, 307–310. doi: 10.1007/s00484-015-1001-2

Sylla, M.B., Faye, A., Giorgi, F., Diedhiou, A. and Kunstmann, H. (2018) Projected heatstress under 1.5 °C and 2 °C global warming scenarios creates unprecedented discomfort for humans in West Africa. *Earth's Future*, 6, 1029–1044. https://doi.org/10.1029/2018EF000873.

Takane, Y., Ohashi, Y., Grimmond, C.S.B., Hara, M. and Kikegawa, Y. (2020) Asian megacity heat stress under future climate scenarios: impact of air-conditioning feedback. *Environemntal Research Communications*, 2, 015004. https://doi.org/10.1088/2515-7620/ab6933.

WMO. (1972) *The Assessment of Human Bioclimate*. Geneva: WMO. Technical note 123, WMO No. 331.

WMO & WHO. (2015) *Heatwaves and Health: Guidance on Warning-System Development*. Geneva: WMO. WMO-No. 1142.

Yang, L., Niyogi, D., Tewari, M., Aliaga, D., Chen, F., Tian, F. and Ni, G. (2016) Contrasting impacts on urban forms on the future thermal environment: example of Beijing metropolitan area. *Environmental Research Letters*, 11, 034018. https://doi.org/10.1088/1748-9326/11/3/034018.

Zou, L. and Zhou, T. (2016) Future summer precipitation changes over CORDEX-East Asia domain downscaled by a regional ocean-atmosphere coupled model: a comparison to the stand-alone RCM. *Journal of Geophysical Research: Atmospheres*, 121, 2691–2704. https://doi.org/10.1002/2015JD024519.

SUPPORTING INFORMATION

Additional supporting information may be found in the online version of the article at the publisher's website.

How to cite this article: Juzbašić, A., Ahn, J.-B., Cha, D.-H., Chang, E.-C., & Min, S.-K. (2022). Changes in heat stress considering temperature, humidity, and wind over East Asia under RCP8.5 and SSP5-8.5 scenarios. *International Journal of Climatology*, 1–17. https://doi.org/10.1002/joc.7636